Journal of Instrumentation

PAPER

Laser blow-off with photodiode detection system at the helically symmetric experiment

To cite this article: J.F. Castillo *et al* 2021 *JINST* **16** P11007

Published by IOP Publishing for Sissa Medialab

Received: *June 15, 2021*
Revised: *October 3, 2021*
Accepted: *October 17, 2021*
Published: *November 9, 2021*

2021 JINST 16 P11007

Laser blow-off with photodiode detection system at the helically symmetric experiment

J.F. Castillo,*[*] C. Clark,[1] A. Bader, K.M. Likin, D.T. Anderson, B. Geiger, S.T.A. Kumar and C. Swee

HSX Plasma Laboratory, University of Wisconsin-Madison, Madison, Wisconsin 53706, U.S.A.

E-mail: jfcastillo@wisc.edu

Abstract: A laser blow-off (LBO) system has been installed in the HSX stellarator to investigate impurity transport. A Nd:YAG laser is used to ablate a target area on a glass slide that has been coated with a thin film of aluminum and rapidly deposits a small, controlled quantity of aluminum atoms into HSX plasma. To study the radial propagation and confinement of the injected aluminum impurities, time-resolved emission measurements are made using a 20 channel AXUV photodiode detection system. The LBO system has achieved its design purpose, most notably the ability to make controlled impurity injection without significant perturbation to the background plasma. A detailed description of the setup as well as initial results of operation are presented.

Keywords: Nuclear instruments and methods for hot plasma diagnostics; Photoemission; Ionization and excitation processes; Detector modelling and simulations II (electric fields, charge transport, multiplication and induction, pulse formation, electron emission, etc)

[1]Currently at Google.
[*]Corresponding author.

https://doi.org/10.1088/1748-0221/16/11/P11007

Contents

2021 JINST 16 P11007

1 Introduction

The presence of impurities in a plasma provides a challenge for fusion reactor relevant devices. Energy loss due to radiation from partially ionized heavy ions can prevent the plasma from reaching the temperatures necessary to sustain fusion. When the impurities accumulate, this can cause a total collapse of the plasma discharge. Impurity transport in a stellarator differs from that in a tokamak in many aspects. Quasi-symmetry provides a bridge between fully 3-D magnetic structure of a traditional stellarator and the 2-D magnetic structure of a tokamak, and HSX is the only operating quasi-symmetric stellarator in the world. In previous experiments, quasi-helical symmetry (QHS) has been shown to reduce neoclassical transport of thermal electrons in HSX [4, 8]. However, the transport of impurity ion species in HSX has not yet been studied. A laser blow-off (LBO) system has been developed for HSX to help determine whether the unique geometrical features of HSX affect the impurity transport as compared to other stellarators. Due to the 3-D nature of the magnetic geometry, small plasma volume, and low plasma density, both injection and emission detection systems have to be carefully designed. Ensuring a maximum signal-to-noise ratio while also avoiding saturation became a priority when developing the detection system.

The LBO technique has been used on a variety of machines, both tokamaks [1, 6, 10] and stellarators [3, 5, 15]. To study a radial propagation and confinement of impurities, the induced radiation is measured along multiple chords with a set of the photodiode arrays. As shown in figure 1, a high power laser illuminates a target area on a glass slide that has been prepared with a thin film of a tracer material on its surface. The tracer material on the slide is ablated, creating a jet composed primarily of neutral atoms that penetrates into the plasma before ionizing. Once the tracer ions are in the plasma, they emit radiation. The radiation from the impurities is monitored and provides information about the transport.

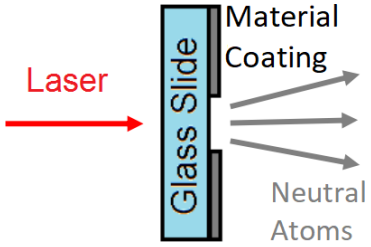

Figure 1. Schematic of the laser-blow off technique. A laser illuminates a thin film of material coating on a glass slide and impurity atoms are injected into the plasma.

LBO is useful for determining impurity transport because it provides the adaptability to choose the impurity species as well as the quantity of impurities injected into the plasma by adjusting the thickness of the tracer film, the spot size of the laser, and the amount of the laser energy density on the target. Control of the quantity of impurity ions deposited into the plasma volume is a distinct advantage of LBO injection over gaseous impurity experiments. Specifically, LBO allows for injecting an amount of impurities that maximizes the signal detected while keeping the injected impurity content to be low enough so that it does not perturb the bulk plasma.

Section 2 describes the laser blow-off section of the diagnostic. Section 3 describes the detector arrays, with a focus on the unique geometric challenges presented by the 3D geometry of HSX. Section 4 presents the justification for choosing aluminum as a tracer material and includes estimations of impurity input into the plasma. Section 5 shows a sample injection along with typical signals from the photodiode arrays. Finally, section 6 provides a brief summary and describes possibilities to improve the diagnostic detection capabilities.

2 Diagnostic setup

The schematic of the LBO system is shown in figure 2. The Continuum Surelight III of the Nd:YAG (wavelength of 1064 nm) is capable of delivering 850 mJ pulse over 4–6 nanoseconds. When the laser is fired, the laser beam travels through two mirrors in the laser housing box and a 50 cm focal length, plano-convex lens. The distance between this lens and the sample determines the area of the sample that is atomized. The beam then travels towards the Brewster's angle window where the majority of the laser light passes through it and a negligible amount of reflected light is transmitted to a power monitor comprised of a photodiode detector. This monitor is a shot-to-shot laser operation diagnostic intended to assure reproducibility when adjusting the lens distance and/or the laser power. The beam travels into a vacuum sample chamber. Held in the middle of this chamber is a $1'' \times 3''$ glass slide that is coated with the tracer material. The glass slide can be moved by two stepper motors in the plane perpendicular to the laser beam axis. When the laser pulse is triggered, it ablates the tracer material and a cloud of neutrals moves down the drift tube towards the vessel port and into the vacuum chamber.

The LBO system is designed to fire the laser once per plasma discharge. After each laser pulse, the stepper motors move the glass slide such that an un-ablated part is exposed to the laser beam for the next pulse. Each glass slide can produce up to 160 impurity injections. Figure 3 shows a top-down picture of the sample chamber where the glass slide is visible. The ablated spots on the

2021 JINST 16 P11007

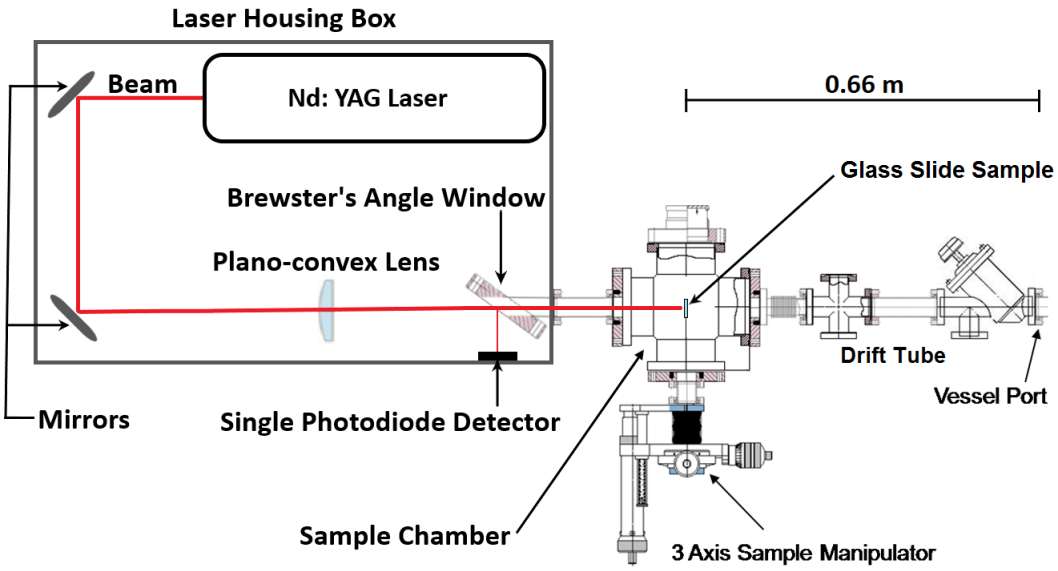

Figure 2. Diagram of the HSX laser blow-off system. The glass slide from figure 1 is placed in the sample chamber shown above and the impurity atoms travel down the drift tube toward the vessel port where they penetrate into the plasma.

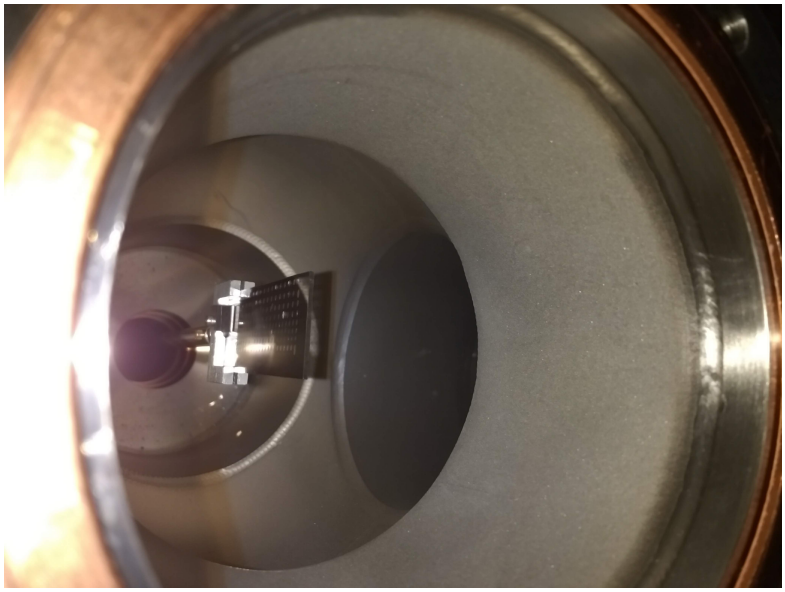

Figure 3. Top-down picture of the sample chamber from figure 2. The spots from the laser ablation are visible on the glass slide.

aluminum film are noticeable. The laser power and spot size can be adjusted after each laser pulse in between plasma discharges.

3 Photodiode detection system

Absolute eXtreme Ultra Violet (AXUV) photodiode pinhole cameras of the AXUV20-EL type (Opto Diode Corp.) are used to measure the radiation emitted by the injected impurities. The detector diodes are specialized to have a uniform response from the ultraviolet up to the soft x-ray energies, covering the spectral range of 0.4 nm to 1100 nm, with an internal quantum efficiency of 100%. The photodiode array has 20 channels corresponding to 20 unique lines-of-sight that view the plasma through a 1 mm pinhole. Custom-built transimpedance amplifiers convert the photo-current into a voltage with gains of up to $2x10^8$ volts per ampere. The total gain of the amplifier board is selectable and adjustments are made during data collection in order to maximize the signal to noise ratio while also avoiding saturation. Optimal amplifier settings may vary under different plasma conditions. Typical signals from these detectors are shown in section 5.

3.1 Systems evaluation

Measurements which validate the array design and verify that individual subsystems have been assembled correctly were taken prior to installation. These measurements tested the entire electrical system of the array with an emphasis on verifying the behavior of the custom amplifiers designed for the project. There are two basic setups used in testing the arrays: one that performs end-to-end functional tests that includes all of the electrical components that will be in the final system, and another setup that only tests the amplifier. It is desirable to perform dedicated tests on the amplifier because it is the most complicated piece of the detection system.

The response test is designed to verify that the frequency response of the amplifier is uniform across the expected range. This test uses a custom signal generator interface board that generates a known current from the voltage waveform on its input and routes it into the amplifier board's connector. The frequency response needs to accurately capture typical rise time signals of the impurity emission on the order of 10 kHz. Since the frequency response is a function of the gain setting, each gain setting is tested separately. There are a total of 8 gain settings selected on the board ranging in values from 2.5×10^5 up to 2×10^8 V/A. Figure 4 shows a Bode plot of the frequency response for gain setting 2×10^7 V/A. All 20 channels are plotted at each excitation frequency (overlapping blue circles), showing that variation between channels is negligible. The red line shows the nominal gain setting. The gain curves for each of the 20 channels show a flat response up to the expected cutoff frequency, the 3 dB down point. The signals presented in this paper are measured using the gain setting from figure 4. It should be noted that the other gain settings also show responses that did not vary from their respective nominal gain. For this reason the board design is considered accurate to specifications.

The noise floor test investigates the background signal that is present even in the absence of stimulation. This provides an idea as to the sensitivity of the setup to ambient electromagnetic interference, and the inherent noise in the amplifier circuit itself. Measurements showed that at high gain, a minimal amount of noise on the signal is expected (~10 mV). These results demonstrated a large signal-to-noise ratio, indicating reliability in the systems performance.

2021 JINST 16 P11007

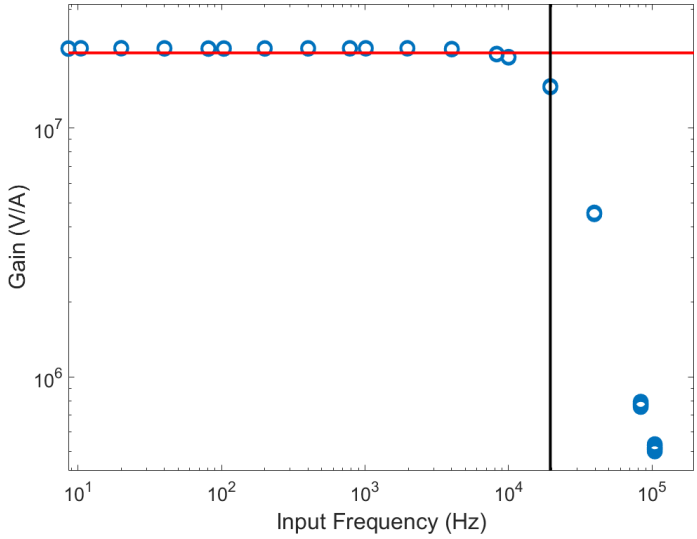

Figure 4. Amplifier frequency response plot for gain setting 2×10^7 V/A. All 20 channels are represented (blue circles) and the red line is the nominal gain.

3.2 Photodiode setup

Five AXUV photodiode arrays are used to measure the radiation emitted by the injected impurities. One array has a filter that transmits high energy soft x-rays and blocks lower energy photons while the other detectors are left unfiltered. Figure 5 illustrates the viewing angle for each camera, each of which defines 20 lines of sight.

Figure 6 shows the top-down view of HSX in relation to the AXUV detector arrays and the beam line port of entry of the LBO drift tube. A12M and A34 are located in two different toroidal positions, the poloidal plane called the 'bean' and the poloidal plane called 'teardrop', respectively. This provides two distinct poloidal plane views to analyze and compare data.

The filtered array, CP34, has the view of the plasma through a 5 µm beryllium foil that filters out the X-ray photons with energy about 1 keV, the upper end of the UV frequency band. These diodes are meant to only measure higher energy soft x-rays, which are only produced from the plasma core where temperatures are high. Experimental results showed that plasma signals from the filtered diode had similar features (such as rise and decay time) as the data from the unfiltered diodes. The filter was then replaced with a 5 µm aluminum oxide foil that filters out the infrared band, the lower end of the UV band. Again, the signals were similar to unfiltered data. Therefore, experimental results support the hypothesis that HSX plasmas produce radiation mostly in the UV frequency band.

In the interest of simplicity, the experimental results presented in this paper focus on one set of AXUV detectors, array A12M, the 'bean' shaped cross-section of the vessel. Figure 7 shows the experimental lines-of-sight (LOS) for each of the 20 photodiode channels surveying the center of the 'bean' view. It is important to point out that channel 11 (green line) has the lowest impact parameter; it passes closest to the plasma core.

2021 JINST 16 P11007

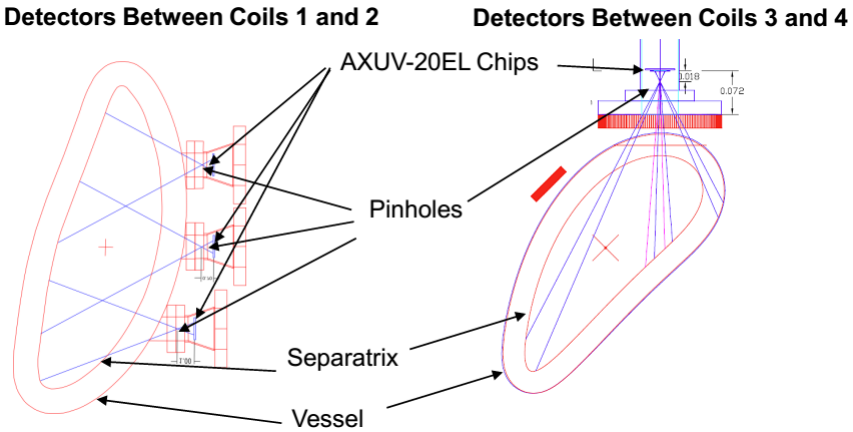

Figure 5. Schematic of the AXUV photodiode arrays. The figure on the left-hand side shows the vessel cross-section, the 'bean' view, where 3 sets of photodiodes chips (top, middle and bottom) detect the plasma emission. The right-hand side shows the vessel cross-section, the 'teardrop' view, monitored by a single chipset. Both cross-sections have sightlines that pass through magnetic axis.

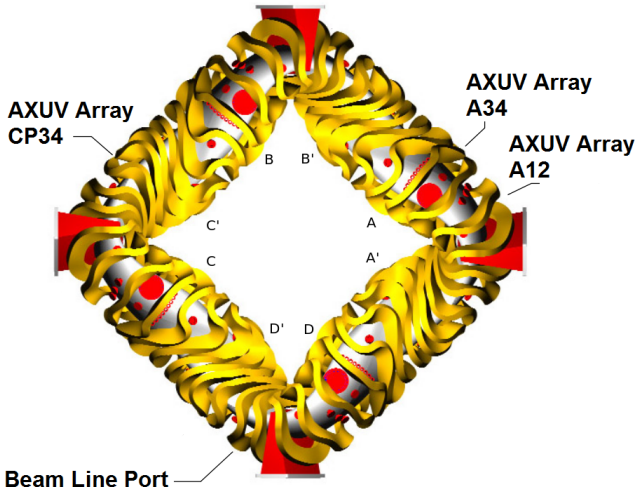

Figure 6. Top-down view of the HSX vessel. This illustrates the physical location of the photodiodes arrays in relation to the injection port.

4 Estimate of neutral ionization location

Various metals have been used in previous and current experiments such as iron [7, 12, 15] and titanium [2]. Aluminum has been used as an LBO tracer element at various experiments [3, 11–13, 15] and a thorough characterization is documented by the laser blow-off system that was designed for use on the French Tokamak TFR [2]. Aluminum was chosen for HSX because it radiates sufficiently to provide a bright photodiode signal at HSX electron temperatures and density, even in low concentrations. Aluminum is also a non-recycling impurity with respect to the HSX vessel walls and is expected to have a low back-scattering probability.

Along with the neutrals, a small fraction of undesirable 'clusters' of aluminum atoms are generated. Clusters are a population of slower, solid, sub-μm bundle of atoms formed during the

2021 JINST 16 P11007

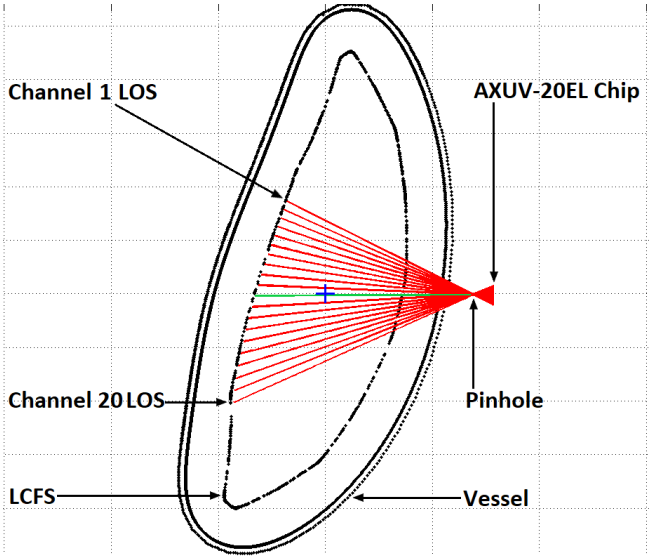

Figure 7. This diagram plots the experimental lines-of-sight of each photodiode detector in the 'bean' view, shown in figure 5. The blue cross represents the magnetic axis of the plasma and the green line represents the chord sightline closest to that axis, channel 11.

vaporization process of the aluminum. These clusters must be avoided because they will act as an additional source of atoms when penetrating into the plasma with a significant temporal delay. Thus, the presence of clusters would make measuring the decay of impurity emissions after LBO injections more challenging and difficult to model. A 10 nm chromium layer between the glass slide and the aluminum layer has been found to be helpful in reducing the amount of clusters injected by the LBO technique by improving the laser absorption and thus increasing energy density [14]. Clusters can also be minimized by applying an optimal energy density on the laser spot of the sample [9].

Following the approach from the experiments cited above, it is found through testing that a 2 µm thick layer of aluminum over a 10 nm chromium layer reduced the generation of clusters. Figure 8 shows a comparison of 2 LBO discharges. The blue signal was generated from a glass slide with a 2 micron thick layer of aluminum whereas the red signal is generated from a 2 micron thick layer of aluminum over a 10 nm chromium layer. The blue signal does not have a pronounced signal peak or a measurable decay, which is characteristic of cluster formation. For this reason, the results presented here use a 2 µm thick layer of aluminum over a 10 nm chromium layer.

Neutrals are deposited in the plasma and the amount of radiation that the impurity will produce once introduced into the plasma must be measurably large. The following calculations provide an estimate of the neutral ionization location by means of simulating the penetration of a beam of neutrals with a characteristic energy spectrum. Knowledge of the spatial distribution of the initial ionization of the injected impurity answers whether or not a measurable fraction of the beam is deposited into the confinement volume. Neutral atoms, in this case aluminum, that enter the vessel encounter plasma in the scrape-off layer (SOL), where the number of ionization events must be acceptably low. In HSX, Langmuir triple probe measurements of the SOL supplement the Thomson scattering data taken in the confinement volume to generate electron temperature (T_e) and density (n_e) profiles (see figure 9).

2021 JINST 16 P11007

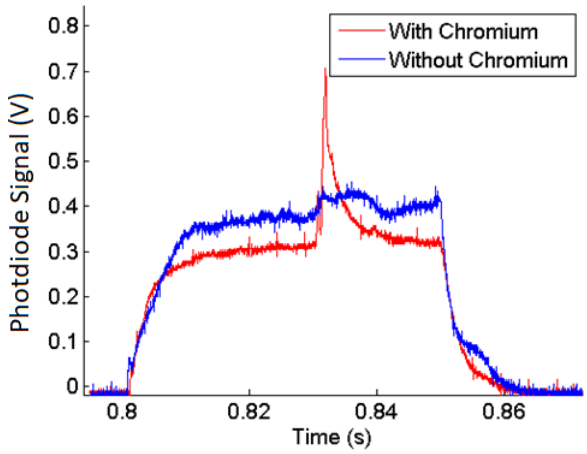

Figure 8. A comparison of 2 LBO discharges. The blue signal was generated from a glass slide with a 2 micron thick layer of aluminum whereas the red signal is generated from a 2 micron thick layer of aluminum over a 10 nm chromium layer.

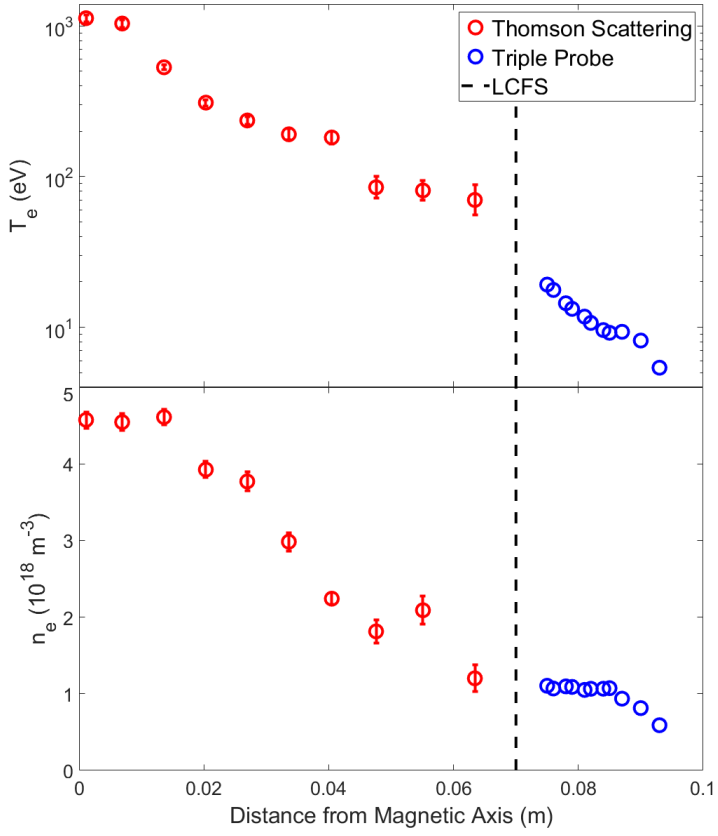

Figure 9. Electron temperature and density profiles taken from a typical 50 kW discharge in HSX. Measurements inside the confinement volume are taken using Thomson scattering and measurements outside are taken using a Langmuir triple probe.

2021 JINST 16 P11007

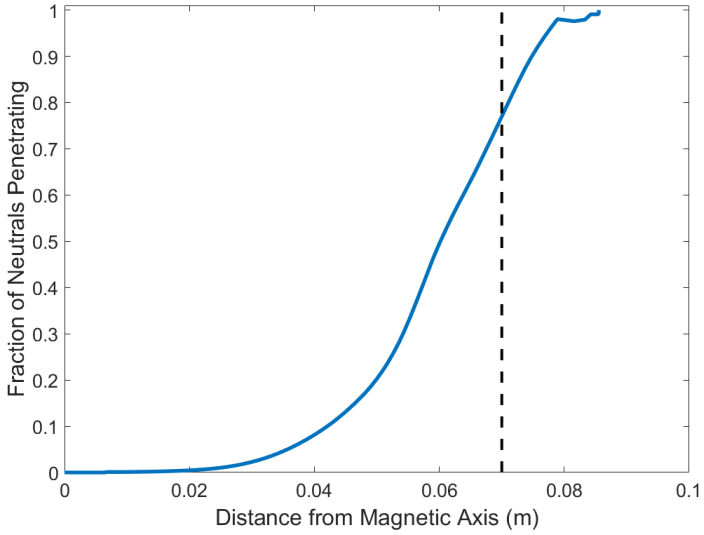

Figure 10. The predicted fraction of an aluminum injection penetrating to various radial locations in HSX. The dashed line represents the last closed flux surface.

Ionization will be dominated by electron impact events, occurring at a rate that is linearly related to the electron density by an ionization coefficient, S_{CD}. This coefficient is a function of electron temperature and the impurity neutrals. The relationship between S_{CD} for aluminum and the electron temperature is found in the Atomic Data and Analysis Structure (ADAS) database.

Impurity confinement experiments require that the impurity ions penetrate into the core plasma. The computation in this paper assumes a constant neutral velocity until the moment of first ionization, after which the ionized impurity ion is affected by the background magnetic field. The initial source distribution is estimated with a simple formula that uses the ionization coefficient S_{CD}, the impurity ion density n_I, and the collision frequency ν. The estimation of the deposition profile of a given portion of the neutral energy spectrum in slab geometry is given by the following equation:

$$n_I(x) = n_{Io} e^{-\frac{1}{\nu}\int_0^x S_{CD} n_e dx} \tag{4.1}$$

Results from equation (4.1) are used to calculate the fraction of neutral aluminum penetrating the plasma as a function of minor radius, represented by the x term in the equation. Other terms needed are the specific plasma minor radius at the actual point of injection (where the distance between the last closed flux surface and the magnetic axis is 7 cm), T_e and n_e measurements, atomic data from ADAS, and the energy of the injected aluminum neutrals when starting at the wall, 2 eV. The energy is estimated using the neutral energy spectrum from the LBO characterization study [2] described in section 4.

Figure 10 is the resulting predicted fraction of an aluminum injection penetrating to various radial locations for the 3D geometry of HSX. These results show the neutral beam projects adequate deposition within confinement volume. Most notably, $\sim$ 80% of the beam neutrals will pass through the scrape-off layer but will be ionized before leaving the confinement volume.

2021 JINST 16 P11007

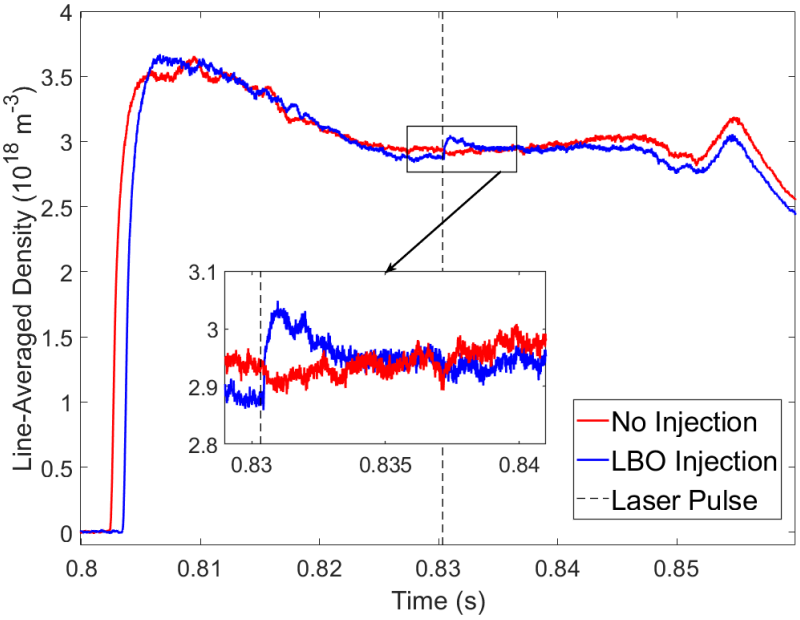

Figure 11. Comparison of line-averaged electron density from plasma discharges with and without LBO impurity injection. The dashed line is the time the laser pulse was triggered.

5 Initial experimental results

A plasma profile of a 1 Tesla QHS discharge, which has 50 kW of ECRH deposited on-axis to a plasma with line-average density of 3×10^{18} m^{-3}, is used in experiments with impurities injected from a glass slide with a 2 μm aluminum layer over a 10 nm chromium layer. The LBO injection creates a transient influx of neutral impurity atoms into the plasma after which the impurities become ionized and are then subject to impurity transport. Once in the plasma, the prominent line radiation emitted by the injected impurities is visible on the photodiodes.

Specific LBO operating parameters such as spot size and laser power effect the photodiode signals from LBO operations. By adjusting the applied laser power on the tracer material and the spot size of the laser beam, a balance of small background plasma perturbations and strong, clean photodiode signals are maintained. An experimental survey was used to determine operating parameters that produce strong photodiode signals, acceptable perturbation to the electron line-averaged density, and little evidence of cluster injection. Figure 11 shows the line-averaged density from an interferometer as a function of time. An inset shows an expanded view of the laser pulse. The effect of the LBO injection on the density is noticeable on the line-averaged density, with the LBO contributing roughly a 5% increase. This is in line with increases seen on other experiments with laser blow-off devices [14].

Figure 12 represents six separate plasma discharges. The gray lines are the individual time traces and the blue lines are the average. The top plot is the emission signal from the channel 11 of the bean view. The middle and bottom represent the line-averaged density and plasma stored energy respectively. The laser is triggered at the dotted line, 0.83033 s. A strong peak and decay of the photodiode signal is observed after the impurity injection while there is minimal perturbation to the density. Measurements for the stored energy also suggest there is no change after the injection.

2021 JINST 16 P11007

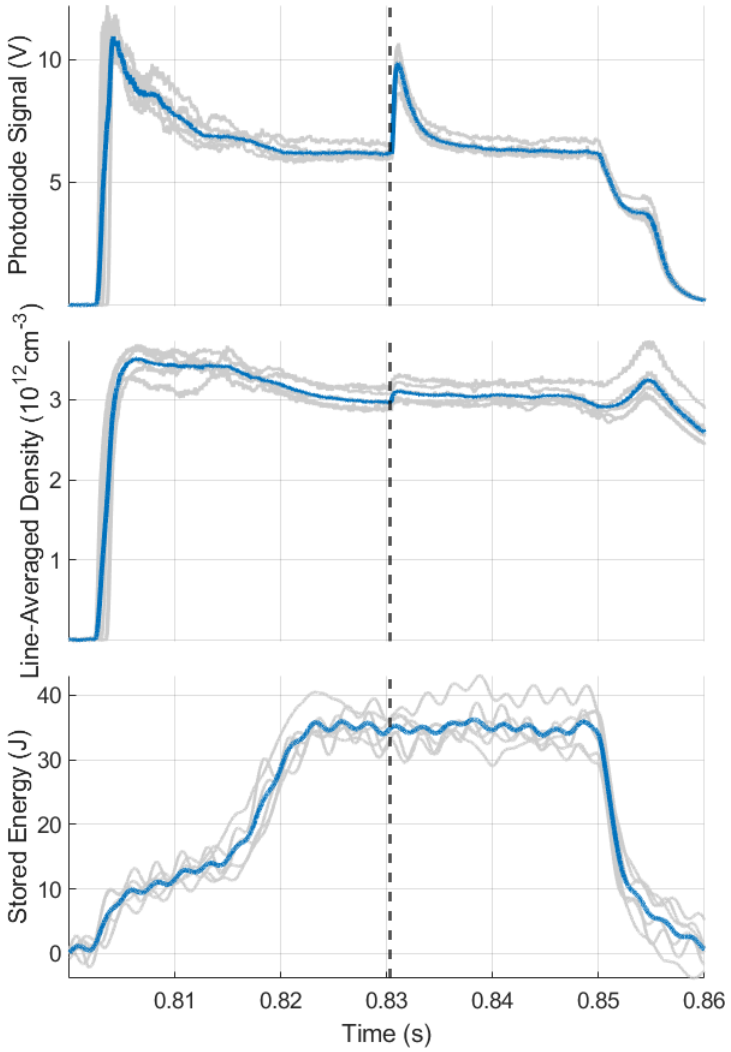

Figure 12. Time traces of (top) the photodiode signal from channel 11 of the bean view shown in figure 7, (middle) the line-averaged density, and (bottom) the plasma stored energy. The gray lines represent six LBO discharges and the blue lines are the average. The dashed line is the time the laser pulse was triggered.

Figure 13 is a 10 ms close-up of a single discharge from figure 12. The line-integrated emission signal shows a clean decay which can be fit by an exponential function $e^{-t/\tau}$ in red. Because the signal can be well fit by a single exponential decay, slower arriving clusters do not significantly contribute to the signal. The emission decay time τ_{imp} for this single LBO discharge is 1.43 ms. This measured decay time is close to the energy confinement time. The six separate plasma discharges from figure 12, where the average decay time is 1.53±0.11 ms, demonstrated good signal reproducibility.

Figure 14 shows a contour plot based on data from 20 channels of the array. The time the plot begins, 0.83033 s, is when the laser is trigger. The most important point of this figure is that signal from all 20 channels can be effectively measured. Data from detector lines-of-sight including, but not exclusive to core measurements, is needed for a complete analysis of impurity transport in a plasma.

2021 JINST 16 P11007

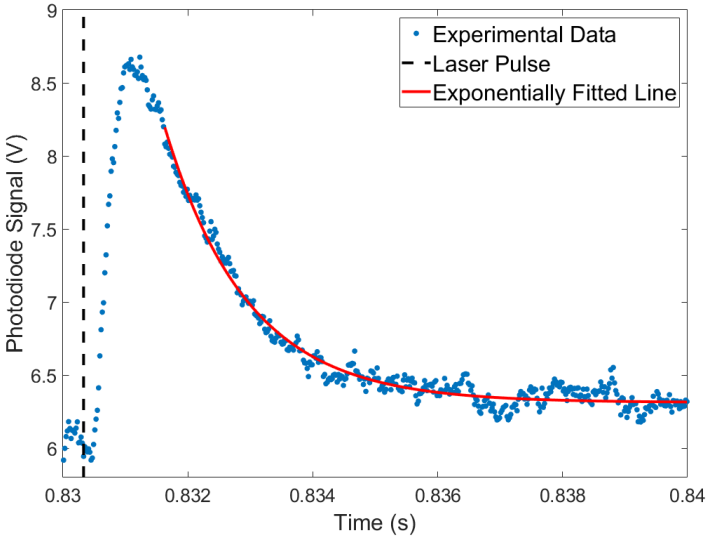

Figure 13. Zoomed-in version of a single discharge from figure 12 for 10 ms. The calculated exponential fit is the red line.

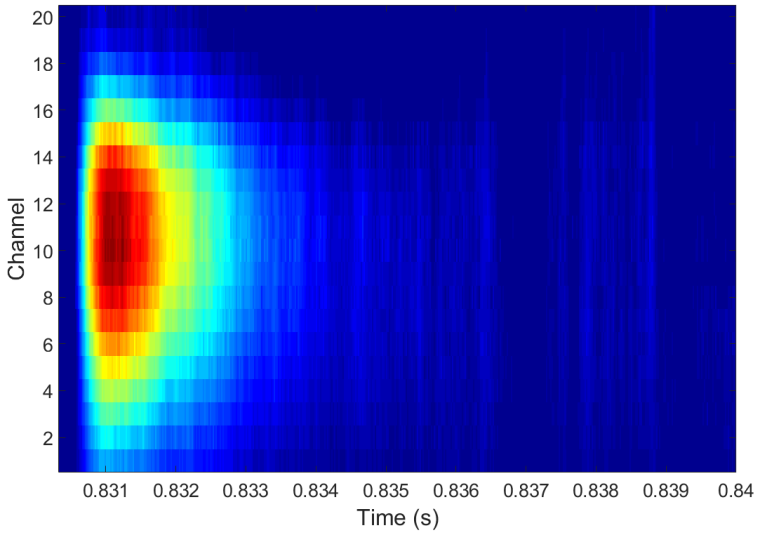

Figure 14. Measured signals of each detector channel as a function of time from the bean view. Channel 11 (between the 10 and 12 tick marks) correlates with the signals plotted in figure 13.

6 Conclusion

The main goal of the LBO system is to characterize the impurity transport on HSX. A detailed description of the laser blow-off diagnostic, including the detector arrays, was provided along with a focus on the unique geometric challenges presented by the 3-D geometry of HSX. The calculated beam penetration of aluminum neutrals showed that there is an adequate deposition of neutrals within the confinement volume. Initial experimental results detected the injection on the photodiode without measuring a substantial change in the electron line-averaged density. The level of impurity transport is determined by experimentally measuring the impurity decay time through integrated emission.

2021 JINST 16 P11007

This paper demonstrated that signal decay measurements can be effectively performed with the current LBO system. Improvements to the diagnostics include a spectroscopy detection system that can measure higher charge state wavelengths, a resonant absorption spectroscopy diagnostic in the LBO drift tube used for characterizing the energy spectrum of the neutrals and the injection of other impurities.

Acknowledgments

This work is supported by the U.S. Department of Energy under Grant DE-FG02-93ER54222.

References

[1] I.L. Beigman, G. Kocsis, A. Pospieszczyk and L.A. Vainshtein, *The line emission of carbon and lithium beams in the plasma edge of TEXTOR*, *Plasma Phys. Control. Fusion* **40** (1998) 1689.

[2] C. Breton, C. de Michelis, W. Hecq and M. Mattioli, *Low energy neutral beam production by laser vaporization of metals*, *Rev. Phys. Appl.* **15** (1980) 1193.

[3] R. Burhenn and A. Weller, *Derivation of local impurity transport quantities from soft-x radiation evolution during tracer injection at W7-AS*, *Rev. Sci. Instrum.* **70** (1999) 603.

[4] J.M. Canik, D.T. Anderson, F.S.B. Anderson, K.M. Likin, J.N. Talmadge and K. Zhai, *Experimental demonstration of improved neoclassical transport with quasihelical symmetry*, *Phys. Rev. Lett.* **98** (2007) 085002.

[5] B. Geiger et al., *Observation of anomalous impurity transport during low-density experiments in W7-X with laser blow-off injections of iron*, *Nucl. Fusion* **59** (2019) 046009.

[6] N.T. Howard, M. Greenwald and J.E. Rice, *Characterization of impurity confinement on Alcator C-Mod using a multi-pulse laser blow-off system*, *Rev. Sci. Instrum.* **82** (2011) 033512.

[7] A. Langenberg et al., *Impurity transport studies at Wendelstein 7-X by means of x-ray imaging spectrometer measurements*, *Plasma Phys. Control. Fusion* **61** (2019) 014030.

[8] J. Lore, *Measurement and transport modeling with momentum conservation of an electron internal transport barrier in HSX*, Ph.D. Thesis, University of Wisconsin-Madison (2010).

[9] D. Manos, *Laboratory study of the PDX/PLT laser blow-off trace element injectors*, *J. Vac. Sci. Tech.* **20** (1982) 1230.

[10] E.S. Marmar, J.L. Cecchi and S.A. Cohen, *System for rapid injection of metal atoms into plasmas*, *Rev. Sci. Instrum.* **46** (1975) 1149.

[11] K. McCormick et al., *New advanced operational regime on the W7-AS stellarator*, *Phys. Rev. Lett.* **89** (2002) 015001.

[12] Y. Nakamura et al., *Plasma performance and impurity behaviour on LHD*, *Nucl. Fusion* **43** (2003) 219.

[13] T. Parisot et al., *Experimental impurity transport and theoretical interpretation in a Tore Supra lower-hybrid heated plasma*, *Plasma Phys. Control. Fusion* **50** (2008) 055010.

[14] B. Zurro et al., *Transport studies using laser blow-off injection of low-Z trace impurities injected into the TJ-II stellarator*, *Nucl. Fusion* **51** (2011) 063015.

[15] B. Zurro et al., *Method to deduce local impurity transport quantities from the evolution of tomographically reconstructed bolometer signals during tracer injection at TJ-II*, *Rev. Sci. Instrum.* **75** (2004) 4231.

2021 JINST 16 P11007